

## Origin of Intense Chiroptical Effects in Undecagold Subnanometer Particles

Makenzie R. Provorse and Christine M. Aikens\*

Department of Chemistry, Kansas State University, Manhattan, Kansas 66506

Received August 13, 2009; E-mail: cmaikens@ksu.edu

**Abstract:** Time-dependent density functional theory (TDDFT) calculations are employed to examine the optical absorption and circular dichroism (CD) spectra of undecagold  $Au_{11}L_4X_2^+$  ( $X = Cl, Br$ ) complexes and their  $Au_2X_2L$  precursors, where L is either 2,2'-bis(diphenylphosphino)-1,1'-binaphthyl (BINAP) or 1,4-diphosphino-1,3-butadiene (dpb). These systems exhibit intense and mirror-image Cotton effects in their CD spectra. Experimental peak positions are well reproduced in the calculations. The low energy peaks of  $Au_{11}L_4X_2^+$  arise primarily from transitions between delocalized metal superatom orbitals. Bidentate phosphine ligands have both a structural and electronic impact on the system. The lowest energy structure of  $Au_{11}L_4X_2^+$  has a chiral  $C_2$  geometry, whereas monodentate phosphine ligands lead to a  $C_1$  structure. In addition, the chiral core structure of  $Au_{11}L_4X_2^+$  is not sufficient to explain the strong Cotton effects, and the intensity of the CD spectrum is increased by the presence of the bidentate phosphine ligands.

### Introduction

Ligand-protected gold nanoparticles have received significant attention in the literature due to important applications in nanotechnology, biology, and catalysis.<sup>1–4</sup> Chiral gold nanoclusters have potential as enantioselective catalysts<sup>5</sup> or in biochemical analysis as electron microscopy labels<sup>6</sup> or in chiral fluorescent assays. Circularly polarized luminescence spectroscopy has previously been employed with quantum dots,<sup>7</sup> and may be utilized in the future with small noble metal nanoparticles. In addition, plasmon-resonance enhanced absorption and circular dichroism studies of DNA are possible due to large electromagnetic fields near noble metal nanoparticles,<sup>8</sup> and silver nanoparticles grown on DNA are suggested to be chiral.<sup>9</sup>

Just over a decade ago, Schaaff and Whetten discovered intense positive and negative Cotton effects in the metal-based electronic transitions in size-selected glutathione-passivated gold nanoparticles.<sup>10,11</sup> At the time, it was not clear whether the dramatic optical activity of the nanoparticles was due to an inherently chiral metal core, a symmetric core that is perturbed by chiral ligands or a chiral adsorption pattern of the ligands,

or the chiral centers in the ligands themselves. Theoretical work on  $Au_{28}(SG)_{16}$  ( $SG =$  glutathione) and  $Au_{14}(MTI)_6$  ( $MTI =$  R-methylthiirane) systems by Beratan et al. using a charge-perturbed particle-in-a-box model and time-dependent density functional theory (TDDFT) calculations supported the hypothesis that a chiral field arising from the adsorbates can induce a chiroptical signature in achiral metal clusters.<sup>12</sup> Alternatively, studies by Garzón et al. suggested that the lowest energy structures of bare gold clusters are disordered and therefore chiral (refs 13, 14, and references therein). The pioneering X-ray structure determination of  $Au_{102}(SR)_{44}$  ( $R =$  *para*-mercapto-benzoic acid) established that the core of this nanoparticle possesses approximate  $C_5$  symmetry even though the passivating ligand itself is achiral (so the crystal structure contains both enantiomers).<sup>15</sup> However, the  $Au_{25}(SR)_{18}^-$  nanoparticle, which was the subject of the original Schaaff and Whetten investigation, has an approximate center of symmetry when  $R =$   $SCH_2CH_2Ph$ <sup>16–18</sup> so it is not chiral and does not display circular dichroism (CD) signals.<sup>19</sup> Lack of a CD spectrum can in general be attributed to an achiral species, a chiral species that rapidly interconverts between enantiomers, or a racemic mixture of enantiomers.

- (1) Link, S.; Beeby, A.; FitzGerald, S.; El-Sayed, M. A.; Schaaff, T. G.; Whetten, R. L. *J. Phys. Chem. B* **2002**, *106*, 3410.
- (2) Smith, R. K.; Nanayakkara, S. U.; Woehle, G. H.; Pearl, T. P.; Blake, M. M.; Hutchison, J. E.; Weiss, P. S. *J. Am. Chem. Soc.* **2006**, *128*, 9266.
- (3) Whetten, R. L.; Price, R. C. *Science* **2007**, *318*, 407.
- (4) Han, J.; Liu, Y.; Guo, R. *J. Am. Chem. Soc.* **2009**, *131*, 2060–2061.
- (5) Takizawa, S.; Patil, M. L.; Marubayashi, K.; Sasai, H. *Tetrahedron* **2007**, *63*, 6512–6528.
- (6) Jahn, W. *J. Struct. Biol.* **1999**, *127*, 106.
- (7) Elliott, S. D.; Moloney, M. P.; Gun'ko, Y. K. *Nano Lett.* **2008**, *8*, 2452–2457.
- (8) Lieberman, I.; Shemer, G.; Fried, T.; Kosower, E. M.; Markovich, G. *Angew. Chem., Int. Ed.* **2008**, *47*, 4855–4857.
- (9) Shemer, G.; Krichevski, O.; Markovich, G.; Molotsky, T.; Lubitz, I.; Kotlyar, A. B. *J. Am. Chem. Soc.* **2006**, *128*, 11006–11007.
- (10) Schaaff, T. G.; Knight, G.; Shafiqullin, M. N.; Borkman, R. F.; Whetten, R. L. *J. Phys. Chem. B* **1998**, *102*, 10643–10646.
- (11) Schaaff, T. G.; Whetten, R. L. *J. Phys. Chem. B* **2000**, *104*, 2630.

- (12) Goldsmith, M.-R.; George, C. B.; Zuber, G.; Naaman, R.; Waldeck, D. H.; Wipf, P.; Beratan, D. N. *Phys. Chem. Chem. Phys.* **2006**, *8*, 63.
- (13) Garzón, I. L.; Reyes-Nava, J. A.; Rodríguez-Hernández, J. I.; Sigal, I.; Beltrán, M. R.; Michaelian, K. *Phys. Rev. B* **2002**, *66*, 073403.
- (14) Santizo, I. E.; Hidalgo, F.; Pérez, L. A.; Noguez, C.; Garzón, I. L. *J. Phys. Chem. C* **2008**, *112*, 17533.
- (15) Jadzinsky, P. D.; Calero, G.; Ackerson, C. J.; Bushnell, D. A.; Kornberg, R. D. *Science* **2007**, *318*, 430.
- (16) Heaven, M. W.; Dass, A.; White, P. S.; Holt, K. M.; Murray, R. W. *J. Am. Chem. Soc.* **2008**, *130*, 3754.
- (17) Akola, J.; Walter, M.; Whetten, R. L.; Häkkinen, H.; Grönbeck, H. *J. Am. Chem. Soc.* **2008**, *130*, 3756.
- (18) Zhu, M.; Aikens, C. M.; Hollander, F. J.; Schatz, G. C.; Jin, R. *J. Am. Chem. Soc.* **2008**, *130*, 5883–5885.
- (19) Wu, Z.; Gayathri, C.; Gil, R. R.; Jin, R. *J. Am. Chem. Soc.* **2009**, *131*, 6535–6542.

Since the initial discovery of gold nanoparticles with significant optical activity, a number of researchers have synthesized other noble metal nanoparticles with a chiral signature. Size-selected gold nanoparticles passivated by D- and L-penicillamine were prepared by Yao et al., and it was determined that their CD spectra display strong and mirror image Cotton effects.<sup>20</sup> Silver nanoparticles with the same ligand exhibit a chiroptical response that is several times larger than that for gold particles, although the core sizes of these nanoparticles may differ.<sup>21</sup> Recently, nanoparticles assigned as a Ag<sub>25</sub> core with 18 glutathione or captopril ligands have been selectively synthesized, and these particles exhibit CD signals with similar orders of magnitudes as the Au<sub>25</sub>(SG)<sub>18</sub><sup>-</sup> nanoparticles of Schaaff and Whetten.<sup>22</sup> Gautier and Bürgi have synthesized N-isobutylcysteine protected gold nanoparticles with strong optical activity; these particles have identical absorption spectra and similar core sizes to the glutathione-passivated nanoparticles of Schaaff and Whetten.<sup>23</sup> Chiral ligands can be exchanged for their opposite enantiomers in thiolate-for-thiolate ligand exchange reactions, which reverses the optical activity of the particles and suggests that the optical activity may be governed by the chiral ligand.<sup>24</sup> Tsukuda et al. synthesized Au<sub>11</sub>(BINAP)<sub>4</sub>X<sub>2</sub><sup>+</sup> (X = Cl or Br, BINAP = 2,2'-bis(diphenylphosphino)-1,1'-binaphthyl) compounds that also display intense and mirror image Cotton effects, whereas compounds stabilized by monodentate phosphine ligands do not.<sup>25</sup> Similar spectra are observed for small 1,1'-binaphthyl-2,2'-dithiol (BINAS)-stabilized nanoparticles.<sup>26</sup>

In general, the relative influences of the ligand and the core structure on nanoparticle chirality and optical activity are not well understood. Few theoretical investigations of chiroptical activity of gold nanoparticles have previously been attempted.<sup>27</sup> The Au<sub>11</sub>(BINAP)<sub>4</sub>X<sub>2</sub><sup>+</sup> system is an ideal compound for a theoretical study of ligand-induced structural changes and metal-metal transitions in the CD spectrum. Undecagold clusters were first synthesized over 40 years ago<sup>28</sup> and are commonly used as biological labels.<sup>6</sup> Several crystal structures have been determined for these particles. Au<sub>11</sub>X<sub>3</sub>(PR<sub>3</sub>)<sub>7</sub> (X = thiolate, halide, or cyano) compounds tend to have incomplete icosahedral skeletons with idealized C<sub>3v</sub> symmetry.<sup>29</sup> The Au<sub>11</sub>(PR<sub>3</sub>)<sub>8</sub>Cl<sub>2</sub><sup>+</sup> cluster has a similar incomplete icosahedral shell, and the two halide ions are attached to two opposite gold atoms on a 5-fold ring.<sup>30</sup> In contrast, the [Au<sub>11</sub>(PMePh<sub>2</sub>)<sub>10</sub>]<sup>3+</sup> cation adopts a centered bicapped square antiprism geometry with idealized D<sub>4d</sub> symmetry.<sup>31</sup> Overall, the variety of structures suggests that the ten surface gold atoms in undecagold compounds are relatively fluxional. Similar fluxionality has also been

suggested for bare gold clusters, because Car-Parrinello molecular dynamics simulations show that the surface Au-Au bonds of Au<sub>34</sub><sup>-</sup> can easily break and reform.<sup>32</sup> In consequence, the geometry of the core for complexes with bidentate phosphine ligands such as BINAP may vary somewhat from complexes with monodentate phosphine ligands.

Electronically, the Au<sub>11</sub> subnanometer particle has 8 valence electrons, which represents a common magic number for "superatom" clusters in which the valence electrons of metal atoms combine to form delocalized S, P, D, etc. orbitals.<sup>33</sup> This electron shell model has recently been employed to explain the stability of several bare and monolayer-protected gold nanoparticles in the <2 nm size regime including Au<sub>11</sub>X<sub>3</sub>(PR<sub>3</sub>)<sub>7</sub>.<sup>34</sup>

## Computational Methods

The Amsterdam Density Functional (ADF) program is used for all calculations.<sup>35</sup> Scalar relativistic effects are included by utilizing the zeroth-order regular approximation (ZORA).<sup>36</sup> The Slater type basis sets employed in the ADF calculations are of polarized triple- $\zeta$  (TZP) quality. In the geometry optimizations, a [1s<sup>2</sup>-4f<sup>14</sup>] frozen core for Au, a [1s<sup>2</sup>-3p<sup>6</sup>] frozen core for Br, a [1s<sup>2</sup>-2p<sup>6</sup>] frozen core for P and Cl, and a [1s<sup>2</sup>] frozen core for C are employed; full core basis sets are utilized in the TDDFT calculations. Geometry optimizations employ the X $\alpha$  local density approximation (LDA) functional. The asymptotically correct statistical average of orbital potentials (SAOP)<sup>37,38</sup> is utilized in TDDFT computations to determine energetics, oscillator strengths, and compositions of excited states. The lowest 200 singlet excited states are evaluated. For Au<sub>2</sub>X<sub>2</sub>BINAP, 400 excited states are calculated. Rotatory strengths are also computed using the RESPONSE module in ADF.<sup>39</sup> The computed rotatory strengths  $R$  are transformed from units of 10<sup>-40</sup> esu<sup>2</sup> cm<sup>2</sup> to  $R_e$  in the experimental units of 10<sup>-3</sup> L cm<sup>-1</sup> mol<sup>-1</sup> (often reported as millidegrees, or mdeg) using the appropriate unit conversions and the equation:<sup>40,41</sup>

$$R_e = \frac{16\pi^2 N_A}{3hc \cdot 10^3 \ln 10} R$$

where  $N_A$  is Avogadro's number and  $c$  is the speed of light. Then, the absorption and circular dichroism spectra are fit with a scaled Gaussian function with a width at half-maximum of 20 nm.

Implicit solvation effects on the geometries and/or spectra of the compounds are considered by employing the conductor-like screening model (COSMO)<sup>42</sup> with parameters for chloroform to account for solvent polarization effects on the orbitals and orbital

- (20) Yao, H.; Miki, K.; Nishida, N.; Sasaki, A.; Kimura, K. *J. Am. Chem. Soc.* **2005**, *127*, 15536.
- (21) Nishida, N.; Yao, H.; Ueda, T.; Sasaki, A.; Kimura, K. *Chem. Mater.* **2007**, *19*, 2831.
- (22) Cathcart, N.; Mistry, P.; Makra, C.; Pietrobon, B.; Coombs, N.; Jelokhani-Niaraki, M.; Kitaev, V. *Langmuir* **2009**, *25*, 5840-5846.
- (23) Gautier, C.; Bürgi, T. *J. Am. Chem. Soc.* **2006**, *128*, 11079.
- (24) Gautier, C.; Bürgi, T. *J. Am. Chem. Soc.* **2008**, *130*, 7077.
- (25) Yanagimoto, Y.; Negishi, Y.; Fujihara, H.; Tsukuda, T. *J. Phys. Chem. B* **2006**, *110*, 11611.
- (26) Gautier, C.; Taras, R.; Gladiali, S.; Bürgi, T. *Chirality* **2008**, *20*, 486.
- (27) Hidalgo, F.; Sánchez-Castillo, A.; Garzón, I. L.; Noguez, C. *Eur. Phys. J. D.* **2009**, *52*, 179-182.
- (28) McPartlin, M.; Mason, R.; Malatesta, L. *Chem. Commun.* **1969**, 334.
- (29) Nunokawa, K.; Onaka, S.; Ito, M.; Horibe, M.; Yonezawa, T.; Nishihara, H.; Ozeki, T.; Chiba, H.; Watase, S.; Nakamoto, M. *J. Organomet. Chem.* **2006**, *691*, 638.
- (30) Schulz-Dobrick, M.; Jansen, M. *Z. Anorg. Allg. Chem.* **2007**, *633*, 2326.
- (31) Copley, R. C. B.; Mingos, D. M. P. *J. Chem. Soc., Dalton Trans.* **1996**, 479.

- (32) Gu, X.; Bulusu, S.; Li, X.; Zeng, X. C.; Li, J.; Gong, X. G.; Wang, L.-S. *J. Phys. Chem. C* **2007**, *111*, 8228.
- (33) de Heer, W. A. *Rev. Mod. Phys.* **1993**, *65*, 611.
- (34) Walter, M.; Akola, J.; Lopez-Acevedo, O.; Jadzinsky, P. D.; Calero, G.; Ackerson, C. J.; Whetten, R. L.; Grönbeck, H.; Häkkinen, H. *Proc. Natl. Acad. Sci. U.S.A.* **2008**, *105*, 9157.
- (35) te Velde, G.; Bickelhaupt, F. M.; Baerends, E. J.; Fonseca Guerra, C.; van Gisbergen, S. J. A.; Snijders, J. G.; Ziegler, T. *J. Comput. Chem.* **2001**, *22*, 931.
- (36) van Lenthe, E.; Baerends, E. J.; Snijders, J. G. *J. Chem. Phys.* **1993**, *99*, 4597.
- (37) Gritsenko, O. V.; Schipper, P. R. T.; Baerends, E. J. *Chem. Phys. Lett.* **1999**, *302*, 199.
- (38) Schipper, P. R. T.; Gritsenko, O. V.; van Gisbergen, S. J. A.; Baerends, E. J. *J. Chem. Phys.* **2000**, *112*, 1344.
- (39) Autschbach, J.; Ziegler, T.; Gisbergen, S. J. A.; Baerends, E. J. *J. Chem. Phys.* **2002**, *116*, 6930.
- (40) Koslowski, A.; Sreerama, N.; Woody, R. W. *In Circular Dichroism: Principles and Applications*, 2nd ed.; Berova, N., Nakanishi, K., Woody, R. W., Eds.; Wiley-VCH: New York, 2000.
- (41) Schellman, J. A. *Chem. Rev.* **1974**, *75*, 323-331.
- (42) Klamt, A.; Schüürmann, G. *J. Chem. Soc., Perkin Trans.* **1993**, *2*, 799.
- (43) Bode, B. M.; Gordon, M. S. *J. Mol. Graphics Mod.* **1998**, *16*, 133-138.

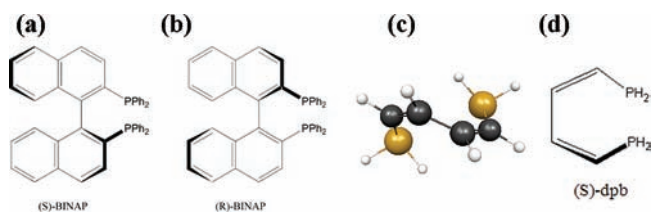


**Figure 1.** (a) Line drawing of (*S*)-BINAP. (b) Line drawing of (*R*)-BINAP. (c) Molecular structure of (*S*)-dpb. (d) Line drawing of (*S*)-dpb.

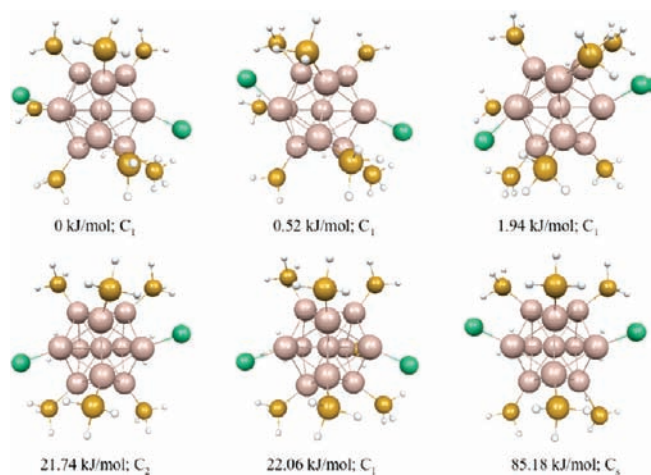


**Figure 2.** Structures, relative energies, and point group symmetries for  $Au_{11}(PH_3)_8Cl_2^+$ . Key: Au, beige; Cl, green; P, orange; H, white; C (not shown), gray.

energies. For the  $Au_2X_2L$  systems, three procedures have been considered including: (1) geometry optimizations and CD spectra computed in the gas phase, (2) optimization in the gas phase followed by TDDFT computations with implicit chloroform, and (3) geometry optimization and TDDFT both using implicit chloroform. For  $Au_{11}L_4X_2^+$ , procedure 2 is employed since optimization in chloroform is found to have negligible effects. MacMolPlt is

employed for molecular structure visualization.<sup>43</sup> The orbitals are plotted using the ADF-GUI program with a contour value of 0.02.

## Results and Discussion

**Model Ligand.** In this study, BINAP, the chiral ligand studied by Tsukuda et al.,<sup>25</sup> is modeled by 1,4-diphosphino-1,3-butadiene (dpb). Both BINAP and dpb contain a 4-carbon chain with alternating double, single, double carbon–carbon bonds (Figure 1). This carbon–carbon bonding structure comes from  $sp^2$ -hybridized orbitals, leaving each carbon with one  $p$  orbital available for pi bonding to the adjacent carbon atoms. Bound to the carbon chain are two  $-PR_2$  moieties (BINAP,  $R = Ph$ ; dpb,  $R = H$ ), so both BINAP and dpb are bidentate phosphine ligands. The lowest energy structure of dpb has a trans configuration of the two double bonds. A second local minimum lies 5.5 kJ/mol in energy higher than the global minimum; this configuration (Figure 1c and d) has the same carbon backbone as BINAP so this isomer is employed in this investigation. The chiral structure of the ligands originates from a twist about the single carbon–carbon bond, creating a nonplanar structure. The R/S enantiomers are defined by the relative orientation of the carbon double bonds, depending on which double bond is above the plane of the molecule and which is below the plane. In this study, the *S* enantiomer of dpb is employed as the chiral ligand bound to undecagold.

**Structures and Relative Energies.  $Au_2X_2L$  ( $X = Cl, Br$ ;  $L = dpb, BINAP$ ).** Computed bond lengths for  $Au_2X_2L$  ( $X = Cl, Br$ ;  $L = dpb, BINAP$ ) in both gas phase and chloroform solvent are presented in the Supporting Information (Table S1). In general, the Au–X bonds increase by 0.02–0.03 Å in solvent, while the Au–P bonds increase by 0.01 Å. The P–C and C–C bond lengths are insensitive to optimization in continuum solvent. The dpb model ligand differs from BINAP most substantially in the carbon–carbon double bond distance, which is approximately 0.08 Å longer in BINAP than in dpb due to resonance in the naphthalene rings. This change in double bond character as well as increased steric crowding lead to an increase of 0.6 Å in the phosphorus–phosphorus distance; however, the

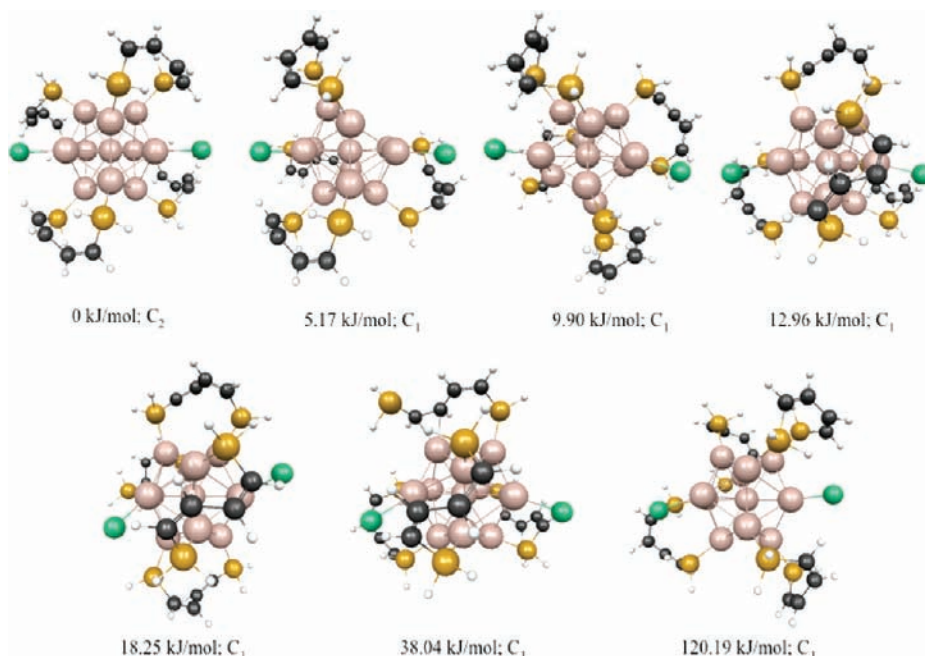


**Figure 3.** Structures, relative energies, and point group symmetries for  $Au_{11}(dpbd)_4Cl_2^+$ . The color scheme is the same as in Figure 2.



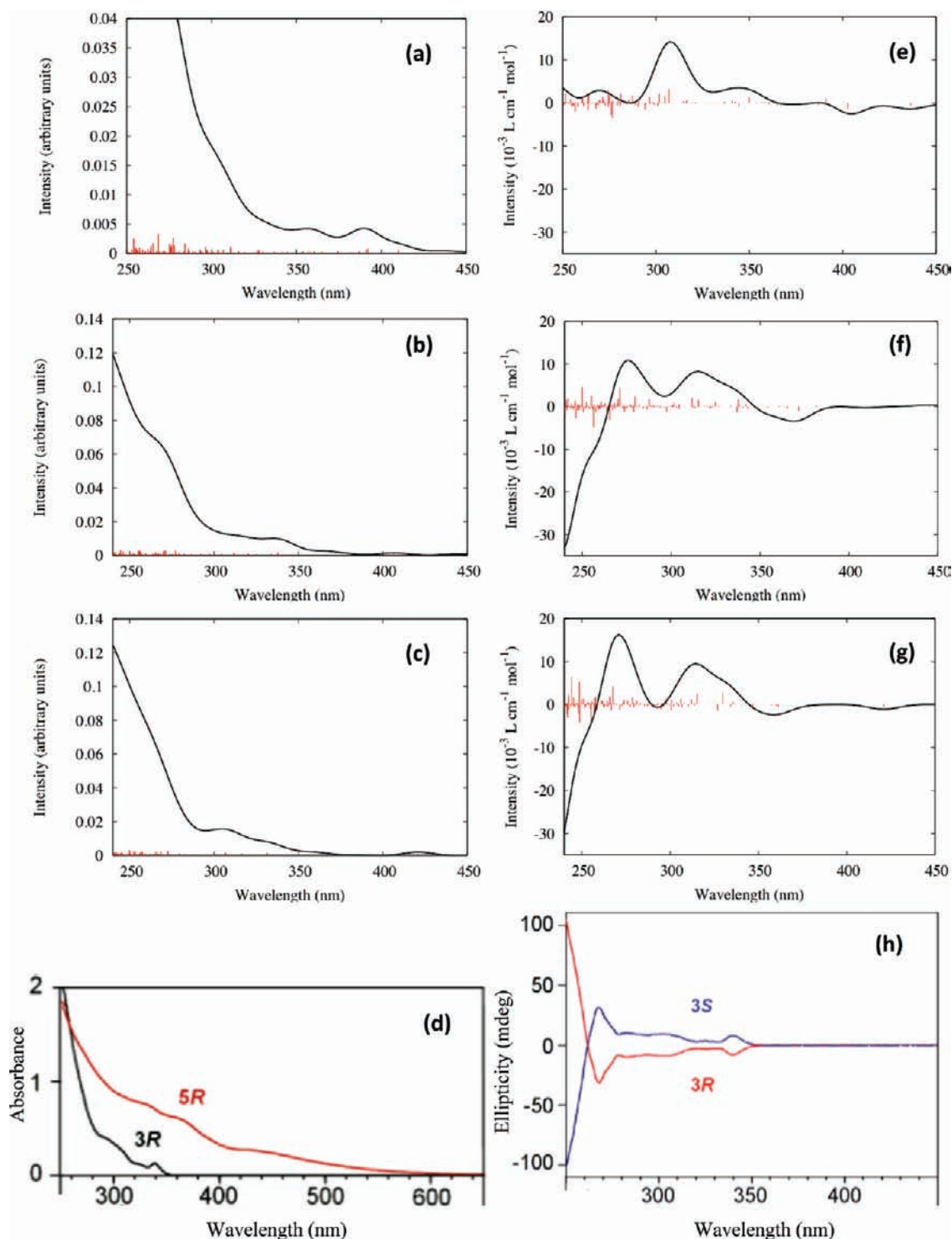


**Figure 4.** Absorption and CD spectra of Au<sub>2</sub>X<sub>2</sub>(S)-BINAP (X = Br, Cl). (a) Theoretical absorption spectrum of Au<sub>2</sub>Br<sub>2</sub>(S)-BINAP in gas phase. (b) Theoretical absorption spectrum of Au<sub>2</sub>Br<sub>2</sub>(S)-BINAP in chloroform. (c) Theoretical absorption spectrum of Au<sub>2</sub>Cl<sub>2</sub>(S)-BINAP in chloroform. (d) Experimental absorption spectrum (3R = Au<sub>2</sub>Br<sub>2</sub>(R)-BINAP) from ref 25, Copyright 2006 American Chemical Society. (e) Theoretical CD spectrum of Au<sub>2</sub>Br<sub>2</sub>(S)-BINAP in gas phase. (f) Theoretical CD spectrum of Au<sub>2</sub>Br<sub>2</sub>(S)-BINAP in chloroform. (g) Theoretical CD spectrum of Au<sub>2</sub>Cl<sub>2</sub>(S)-BINAP in chloroform. (h) Experimental CD spectrum (3R/3S = Au<sub>2</sub>Br<sub>2</sub>(R/S)-BINAP) from ref 25, Copyright 2006 American Chemical Society.

Au–Au bond length is essentially insensitive to the P–P distance. Thus, substitution of BINAP by dpb is not expected to change the predicted Au–Au lengths in the undecagold system.

**Undecagold with Nonchiral Ligand (-PH<sub>3</sub>).** The three lowest energy structures of Au<sub>11</sub>(PH<sub>3</sub>)<sub>8</sub>Cl<sub>2</sub><sup>+</sup> have C<sub>1</sub> symmetry with disordered gold cores (Figure 2). These structures are very close in energy, within a 2 kJ/mol range. A structure with C<sub>2</sub>

symmetry has a much higher relative energy (22 kJ/mol). The structure has a C<sub>2</sub> axis of rotation through the central gold atom. At an even higher relative energy (85 kJ/mol), a nonchiral structure exists with C<sub>s</sub> symmetry. This structure has a mirror plane through the central gold atom, the capping gold atom, and one gold atom of the 5-membered ring.

**Undecagold with Chiral Ligand (dpb).** Four dpb ligands are bound to undecagold through eight surface atoms. The possible

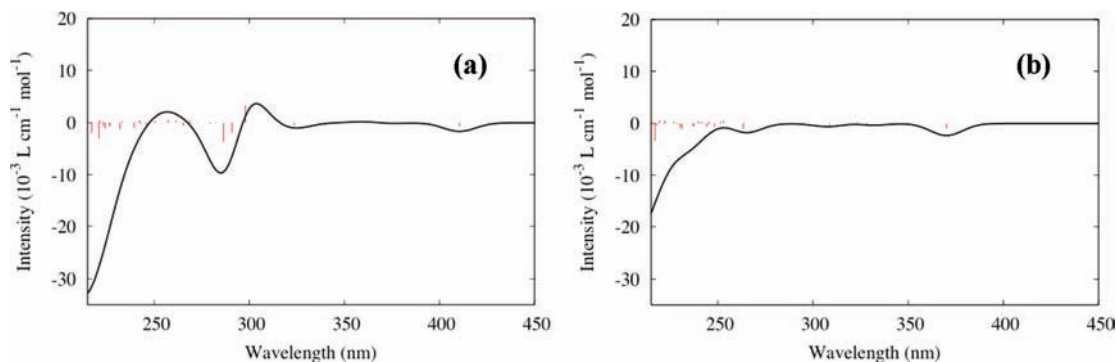


**Figure 5.** CD spectra of S enantiomer of  $\text{Au}_2\text{X}_2\text{dpb}$  ( $\text{X} = \text{Br}, \text{Cl}$ ). (a) Theoretical CD spectrum of  $\text{Au}_2\text{Br}_2\text{dpb}$ . (b) Theoretical CD spectrum of  $\text{Au}_2\text{Cl}_2\text{dpb}$ .

**Table 1.** Transitions Responsible for the Primary Peaks above 250 nm in the CD Spectrum of  $\text{Au}_2\text{X}_2\text{dpb}$

state	wavelength (nm)	oscillator strength	rotatory strength ( $10^{-40}$ esu $^2$ cm $^2$ )	transition from occupied orbital	transition to unoccupied orbital	weight	transition dipole moment (electric)			total magnetic dipole moment			
							X	Y	Z	X	Y	Z	
$\text{Au}_2\text{Br}_2\text{dpb}$	6	298	0.003	77.412	145 (HOMO)	147 (LUMO+1)	0.530	-1.004	0.659	0.006	-0.0654	1.8889	0.0054
					140 (HOMO-5)	146 (LUMO)	0.390	1.196	-0.092	-0.010			
	7	291	0.019	-43.323	145 (HOMO)	148 (LUMO+2)	0.564	-0.527	0.210	0.004	-0.3368	0.3390	0.0023
					140 (HOMO-5)	146 (LUMO)	0.241	0.930	-0.071	-0.008			
					145 (HOMO)	147 (LUMO+1)	0.128	0.487	-0.320	-0.003			
	8	286	0.060	-86.017	145 (HOMO)	148 (LUMO+2)	0.380	0.430	-0.171	-0.003	-0.3285	0.4517	-0.0004
					145 (HOMO)	147 (LUMO+1)	0.252	0.679	-0.445	-0.004			
					140 (HOMO-5)	146 (LUMO)	0.172	0.778	-0.060	-0.007			
	$\text{Au}_2\text{Cl}_2\text{dpb}$	6	281	0.013	-0.241	139 (HOMO-6)	146 (LUMO)	0.878	0.010	-0.004	1.662	-0.0049	0.0014
122 (HOMO-5)						128 (LUMO)	0.630	1.420	-0.041	0.006	-0.2101	2.1128	0.0040
7		271	0.010	0.355	127 (HOMO)	129 (LUMO+1)	0.190	-0.759	0.345	0.003			
					127 (HOMO)	130 (LUMO+2)	0.733	0.778	-0.123	-0.002	0.1912	0.4255	0.0009
					127 (HOMO)	129 (LUMO+1)	0.199	-0.762	0.347	0.003			
8		264	0.018	3.694	121 (HOMO-6)	128 (LUMO)	0.864	-0.002	0.003	-1.572	0.0150	0.0284	-0.0400
					127 (HOMO)	129 (LUMO+1)	0.488	1.179	-0.537	-0.004	-0.2513	-0.4163	-0.0039
9		263	0.099	-26.033	127 (HOMO)	130 (LUMO+2)	0.219	0.419	-0.066	-0.001			

structures are limited by the bond lengths and angles of dpb and steric interference by the chloride ligands. As a result, seven structures are possible for  $\text{Au}_{11}(\text{dpb})_4\text{Cl}_2^+$ . The lowest energy structure has a  $C_2$  axis of rotation through the central gold atom, creating a symmetrical gold core (Figure 3). Unlike the  $-\text{PH}_3$  lowest energy structure, the chloride ligands are directly opposite each other in a linear fashion and both the dpb and chloride ligands are superimposable after a  $180^\circ$  rotation about the  $C_2$  axis. The higher energy  $\text{Au}_{11}(\text{dpb})_4\text{Cl}_2^+$  clusters, with relative energies ranging from 5 to 120 kJ/mol, have  $C_1$  symmetry due to the lack of mirror planes or axes of rotation present in the structures.

**Absorption and Circular Dichroism Spectra.  $\text{Au}_2\text{X}_2\text{L}$  ( $\text{X} = \text{Cl}, \text{Br}$ ;  $\text{L} = \text{dpb}, \text{BINAP}$ ).** The  $\text{Au}_2\text{Br}_2\text{BINAP}$  absorption and CD spectra calculated in this work are shown in Figure 4 along with the experimental data of Tsukuda et al.<sup>25</sup> The absorption spectra of  $\text{Au}_2\text{Br}_2\text{BINAP}$  both in the gas phase (Figure 4a) and in implicit chloroform (Figure 4b) have the same general shape as the experimental spectrum (Figure 4d). The spectrum calculated in chloroform has one peak at about 340 nm, in agreement with experiment. However, the spectrum calculated in gas phase has two peaks at higher wavelengths (about 360 and 390 nm) than the characteristic peak found in experiment. The CD spectrum of  $\text{Au}_2\text{Br}_2\text{BINAP}$  calculated in chloroform (Figure 4f) has a large negative peak at about 240 nm and a smaller positive peak at about 275 nm. These peaks agree with experiment (Figure 4h), which has a large negative peak at about 250 nm and a smaller positive peak at about 270 nm. The theoretical and experimental spectra also display a series of small

positive peaks for wavelengths up to 350 nm. Although some differences in intensities are evident, the overall agreement is quite good. However, when solvent effects on the Kohn–Sham orbitals and orbital energies are not taken into account, the gas phase CD spectrum (Figure 4e) has a small positive peak at 250 nm instead of the large negative peak found in experiment. Clearly, solvent effects must be included to calculate reasonable CD spectra; therefore, all subsequent spectra include these effects.

Exchanging bromide ligands for chloride ligands does not significantly alter the shape of the absorption or CD spectrum (Figure 4c and g, respectively). The absorption spectrum of  $\text{Au}_2\text{Cl}_2\text{BINAP}$  has a peak around 340 nm and is in good agreement with the absorption spectrum of  $\text{Au}_2\text{Br}_2\text{BINAP}$ , although it is slightly shifted to shorter wavelengths by about 5 nm. The CD spectrum of  $\text{Au}_2\text{Cl}_2\text{BINAP}$  has a large negative peak at about 235 nm and a smaller positive peak at about 270 nm. Compared to the CD spectrum of  $\text{Au}_2\text{Br}_2\text{BINAP}$ , the large negative peak is shifted to a lower wavelength by about 5 nm, similar to the absorption spectra. The small positive peak is in very good agreement with that of  $\text{Au}_2\text{Br}_2\text{BINAP}$ .

When the model ligand, dpb, is employed instead of BINAP, the CD spectrum is altered (Figure 5).  $\text{Au}_2\text{Br}_2\text{dpb}$  has a CD spectrum with a large negative peak shifted 35 nm to a smaller wavelength (at about 215 nm) and a smaller peak with the opposite sign as experiment shifted 15 nm to higher wavelength (at about 285 nm).  $\text{Au}_2\text{Cl}_2\text{dpb}$  has a similar large negative peak at 200 nm and a much smaller opposite signed peak as experiment at 260 nm. The general shape of the CD spectra is

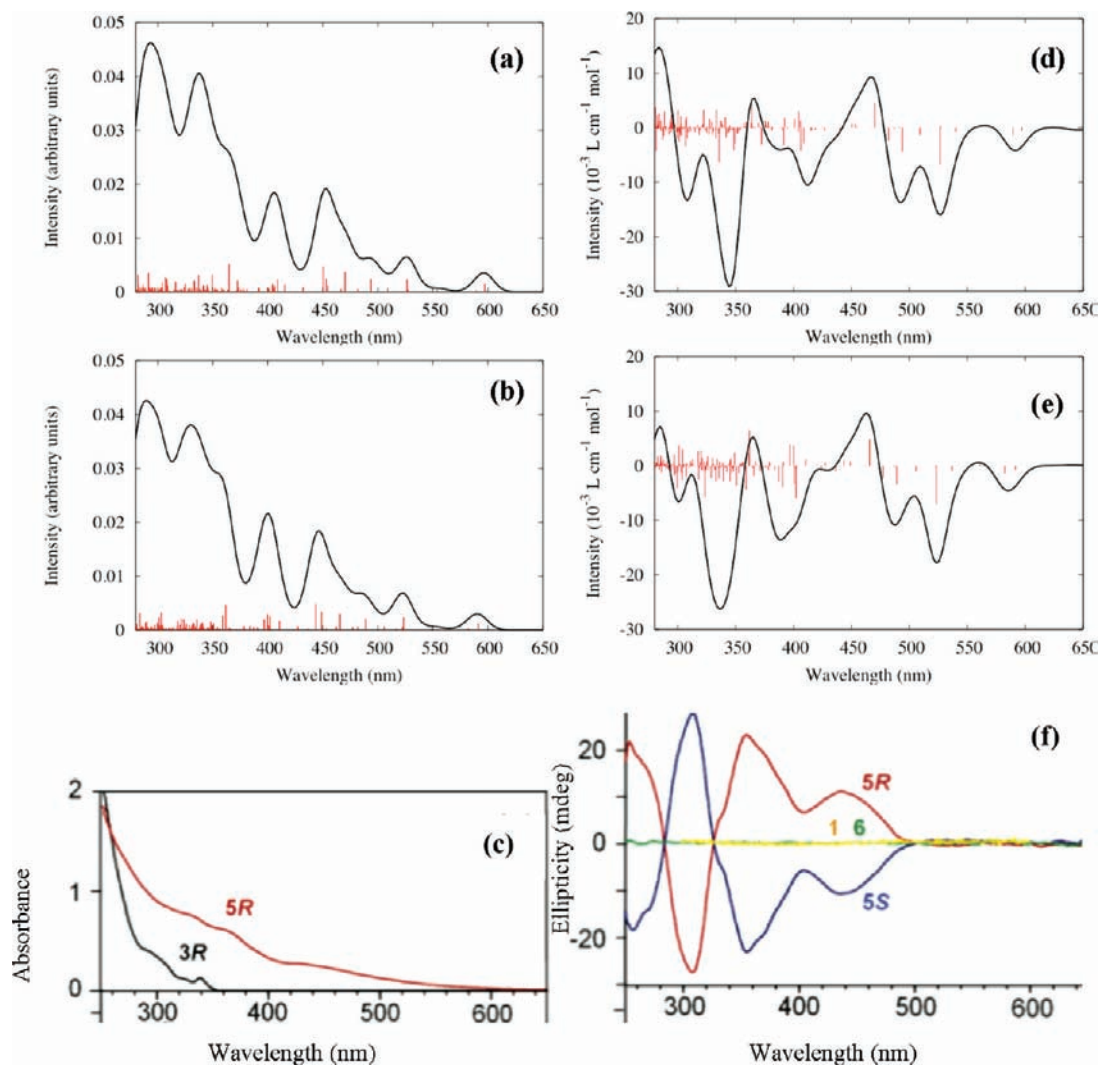


**Figure 6.** Absorption and CD spectra of  $\text{Au}_{11}((S)\text{-dpb})_4\text{X}_2^+$  ( $\text{X} = \text{Br}, \text{Cl}$ ). (a) Theoretical absorption spectrum of  $\text{Au}_{11}((S)\text{-dpb})_4\text{Br}_2^+$ . (b) Theoretical absorption spectrum of  $\text{Au}_{11}((S)\text{-dpb})_4\text{Cl}_2^+$ . (c) Experimental absorption spectrum (5R =  $\text{Au}_{11}((R)\text{-BINAP})_4\text{Br}_2^+$ ) from ref 25, Copyright 2006 American Chemical Society. (d) Theoretical CD spectrum of  $\text{Au}_{11}((S)\text{-dpb})_4\text{Cl}_2^+$ . (e) Theoretical CD spectrum of  $\text{Au}_{11}((S)\text{-dpb})_4\text{Br}_2^+$ . (f) Experimental CD spectrum (5R/5S =  $\text{Au}_{11}((R/S)\text{-BINAP})_4\text{Br}_2^+$ ) from ref 25, Copyright 2006 American Chemical Society.

**Table 2.** Location of Features in the  $\text{Au}_{11}\text{L}_4\text{Br}_2^+$  CD Spectrum

experimental data (ref 25)			theoretical data			
nm	shape <sup>a</sup>	eV	state	$R$ ( $10^{-40}$ esu <sup>2</sup> cm <sup>2</sup> )	computed (eV)	scaled <sup>b</sup> (eV)
435	(br)	2.851	8	-157	2.355	2.705
			11	-101	2.511	2.861
			14	-54	2.573	2.923
403	(dip)	3.077	15	105	2.637	2.987
			20	-17	2.819	3.169
388	(sh)	3.196	22	-14	2.906	3.256
			27	-66	3.033	3.383
			29	-98	3.052	3.402
354	(s)	3.503	37	-74	3.167	3.517

<sup>a</sup> br: broad; dip: dip in peak intensity; sh: shoulder; s: strong peak

<sup>b</sup> Computed energies plus 0.35 eV.

consistent for both  $\text{Au}_2\text{Br}_2\text{dpb}$  and  $\text{Au}_2\text{Cl}_2\text{dpb}$  complexes with a large negative peak, similar to experiment, and a smaller peak that has the opposite sign as experiment. Thus in the subsequent  $\text{Au}_{11}(\text{dpb})_4\text{X}_2^+$  calculations, replacement of BINAP by the model ligand dpb is expected to affect the CD spectrum at wavelengths shorter than 350 nm.

In the  $\text{Au}_2\text{Br}_2\text{dpb}$  spectrum, the first five peaks arise from transitions out of the five highest-lying orbitals (primarily halide

$p$  orbitals) into the lowest unoccupied orbital. These five peaks have very small oscillator ( $f < 0.01$  au) and rotatory ( $|R| < 20 \times 10^{-40}$  esu<sup>2</sup> cm<sup>2</sup>) strengths. As can be seen from Table 1, the types of transitions responsible for the peaks in the CD spectra of  $\text{Au}_2\text{Br}_2\text{dpb}$  and  $\text{Au}_2\text{Cl}_2\text{dpb}$  are equivalent, although for  $\text{Au}_2\text{Cl}_2\text{dpb}$  some of the mixed positive and negative contributions offset so only the peak at 263 nm is apparent in the CD spectrum.

**$\text{Au}_{11}(\text{dpb})_4\text{X}_2^+$  ( $\text{X} = \text{Cl}, \text{Br}$ ).** Experimentally, the circular dichroism spectra of  $\text{Au}_{11}(\text{BINAP})_4\text{X}_2^+$  are essentially identical for  $\text{X} = \text{Cl}$  and  $\text{Br}$ .<sup>25</sup> The calculated absorption and CD spectra of  $\text{Au}_{11}(\text{dpb})_4\text{X}_2^+$  from this work are shown in Figure 6 with the experimental  $\text{Au}_{11}(\text{BINAP})_4\text{Br}_2^+$  results from ref 25. In the experimental absorption spectrum of  $\text{Au}_{11}(\text{BINAP})_4\text{Br}_2^+$  (Figure 6c), some absorption is evident above 500 nm. The intensity of the absorption grows as the wavelength decreases, and slight peaks or shoulders are noticeable at 430, 370, and 340 nm. In the theoretical absorption spectrum of  $\text{Au}_{11}(\text{dpb})_4\text{Br}_2^+$  (Figure 6a), the absorption increases with decreasing wavelength, and several peaks are evident in the fitted spectrum at wavelengths similar to those observed in experiment. For example, the



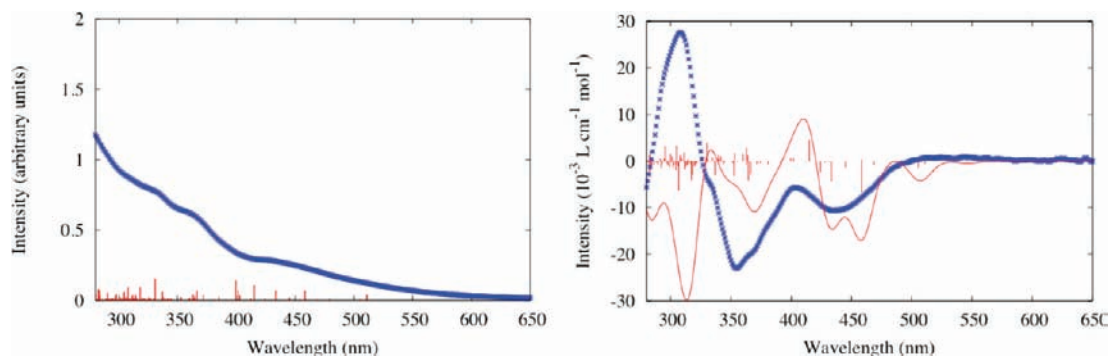


**Figure 7.** Absorption (a) and CD (b) spectra of  $\text{Au}_{11}\text{L}_4\text{Br}_2^+$ . Experimental data for  $\text{L} = \text{S-BINAP}$  (ref 25) are shown in blue crosses. Theoretical data for  $\text{L} = \text{S-dpb}$  are shifted by 0.35 eV and shown in solid red. In (a), the theoretical data are scaled by a factor of 30 relative to Figure 6a.

theoretical peak at 450 nm appears to correlate with the broad experimental peak at 430 nm.

The experimental CD spectrum (Figure 6f) for the S complex has two strong negative peaks at 440 and 360 nm and an intense positive peak at 310 nm. In the theoretical  $\text{Au}_{11}(\text{dpb})_4\text{Br}_2^+$  and  $\text{Au}_{11}(\text{dpb})_4\text{Cl}_2^+$  spectra (Figures 6d and 6e), the first negative peak occurs about 480–530 nm and the second negative peak is positioned at 390–410 nm. These values are within the accuracy typically expected for TDDFT. It has been observed previously that metal–metal transitions in  $\text{Au}_{25}(\text{SR})_{18}^-$  are underestimated by about 0.15–0.20 eV.<sup>44,45</sup> In addition, substitution of BINAP by the model ligand could potentially lead to an additional red-shift in predicted wavelengths. As shown in Table 2, offsetting the theoretically predicted peaks by 0.35 eV leads to good agreement with the experimental data for the main features above 340 nm; the offset theoretical data are presented in Figure 7 with the experimental data from ref 25. It should be noted that the third broad peak in the theoretical CD spectrum is negative, whereas the corresponding peak in the experimental spectrum is positive. This peak lies in the <350 nm region where, as discussed in the preceding section, the differences in BINAP and dpb ligand absorption play a significant role.

Kohn–Sham orbitals involved in low-energy excitations of  $\text{Au}_{11}(\text{dpb})_4\text{Cl}_2^+$  are shown in Figure 8. The HOMO, HOMO-1, and HOMO-2 are essentially superatom P orbitals. The HOMO lies 0.31 eV higher in energy than the HOMO-1 and 0.44 eV higher in energy than the HOMO-2, so these orbitals are not nearly degenerate unlike the P orbitals in  $\text{Au}_{25}(\text{SH})_{18}^-$ ,<sup>44</sup> where the range of orbital energies is only 0.03 eV. The ten occupied orbitals below HOMO-2 with orbital energies from  $-9.793$  to  $-10.383$  eV are a mixture of Cl *p* and Au *d* orbitals. The LUMO, LUMO+1, LUMO+3, LUMO+6, LUMO+7, and LUMO+9 have significant superatom D character, while LUMO+2, LUMO+4, LUMO+5, and LUMO+8 are primarily  $\pi^*$  orbitals on the dpb ligands. In addition to the twist of the axes of the superatom P and D orbitals, there is also a twist within the individual lobes of these orbitals.

The wavelengths, rotatory strengths, and single-particle transitions and their weightings are presented in Tables 3 and S2 (see Supporting Information for Table S2) for the primary excitations responsible for the CD spectrum. As shown in Table 3, the excitations generally arise from transitions out of a metal-based P orbital into a metal-based D orbital. Overall, the two large negative peaks in the CD spectrum at longer wavelengths

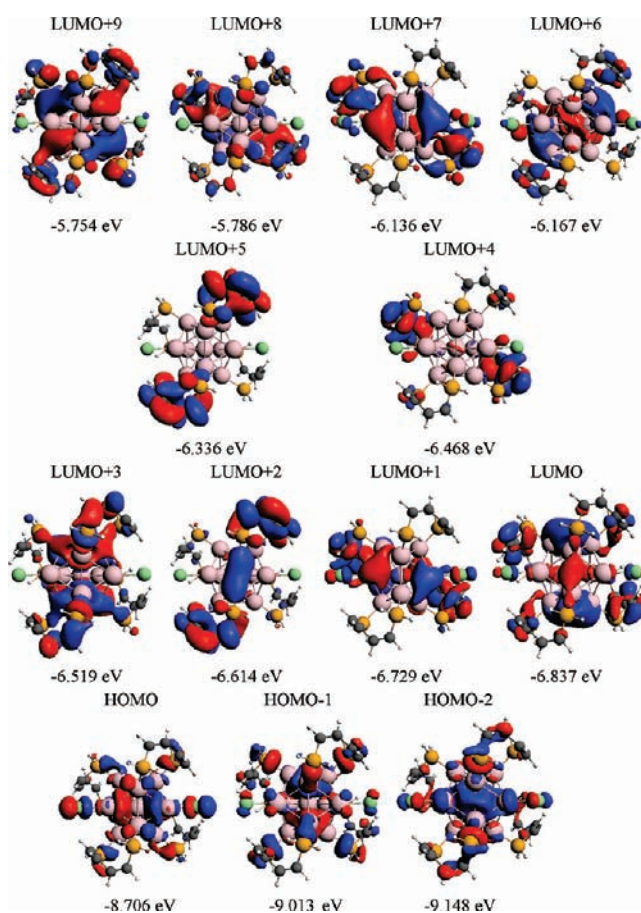


**Figure 8.** Kohn–Sham orbitals involved in low-energy excitations of  $\text{Au}_{11}(\text{dpb})_4\text{Cl}_2^+$ .

are chiefly caused by excitations within the metal core. In addition to significant metal–metal transition character, a few peaks also have excitations into the LUMO+2 and LUMO+4 that involve metal-to-ligand charge transfer transitions. Although the weight of these states is generally small, the inability of TDDFT to properly treat charge-transfer transitions could affect the location or intensity of some of these peaks.

Replacement of the bidentate ligand dpb by the monodentate ligand  $\text{PH}_3$  has a significant effect on the CD spectrum. The  $\text{Au}_{11}(\text{dpb})_4\text{Cl}_2^+$  states at 523 nm ( $R = -160.5 \times 10^{-40} \text{ esu}^2 \text{ cm}^2$ ) and 362 nm ( $R = 149.9$ ) have over twice the rotatory strength of the strongest peaks in the CD spectrum of the lowest energy structure of  $\text{Au}_{11}(\text{PH}_3)_3\text{Cl}_2^+$  (Figure 9a). The strongest peaks

(44) Aikens, C. M. *J. Phys. Chem. C* **2008**, *112*, 19797–19800.

(45) Aikens, C. M. *J. Phys. Chem. A* **2009**, *113*, 10811–10817.

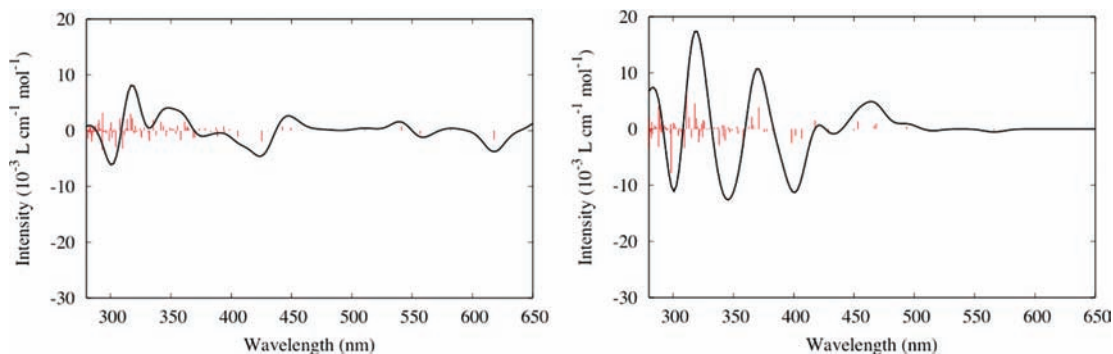


**Figure 9.** Theoretical CD spectrum of  $\text{Au}_{11}(\text{PH}_3)_8\text{Cl}_2^+$ . (a) Lowest energy  $C_1$  structure. (b) Structure with  $C_2$  symmetry (21.74 kJ/mol above minimum energy structure).

**Table 3.** Primary Excitations Responsible For the  $\text{Au}_{11}(\text{dpb})_4\text{Cl}_2^+$  CD Spectrum<sup>a</sup>

state	peak energy (eV)	wavelength (nm)	rotatory strength ( $10^{-40}$ esu <sup>2</sup> cm <sup>2</sup> )	transition from occupied orbital	transition to unoccupied orbital	weight
7	2.369	523	-160	574(HOMO-1)	576 (LUMO)	0.4891
				575 (HOMO)	580(LUMO+4)	0.1772
				573(HOMO-2)	577(LUMO+1)	0.1201
				573(HOMO-2)	576 (LUMO)	0.1037
11	2.535	489	-78	573(HOMO-2)	577(LUMO+1)	0.5922
				574(HOMO-1)	580(LUMO+4)	0.1845
14	2.598	477	-52	573(HOMO-2)	578(LUMO+2)	0.4231
				575 (HOMO)	583(LUMO+7)	0.3951
15	2.663	466	110	574(HOMO-1)	579(LUMO+3)	0.1204
				575 (HOMO)	582(LUMO+6)	0.4118
				574(HOMO-1)	580(LUMO+4)	0.1709
				573(HOMO-2)	579(LUMO+3)	0.1507
26	3.083	402	-137	573(HOMO-2)	577(LUMO+1)	0.1316
				573(HOMO-2)	583(LUMO+7)	0.4114
28	3.094	401	-77	575 (HOMO)	585(LUMO+9)	0.2392
				571(HOMO-4)	576 (LUMO)	0.1148
29	3.100	400	85	573(HOMO-2)	582(LUMO+6)	0.5118
				572(HOMO-3)	582(LUMO+6)	0.2984
30	3.125	397	90	575 (HOMO)	585(LUMO+9)	0.4617
				573(HOMO-2)	583(LUMO+7)	0.2230
				572(HOMO-3)	577(LUMO+1)	0.3669
				573(HOMO-2)	582(LUMO+6)	0.3029
				571(HOMO-4)	576 (LUMO)	0.1747

<sup>a</sup> See Table S2 in the Supporting Information for states with wavelengths below 395 nm.

for  $\text{Au}_{11}(\text{PH}_3)_8\text{Cl}_2^+$  include the ones at 618 nm ( $R = -37.1$ ), 425 nm ( $R = -43.8$ ), 361 nm ( $R = 36.8$ ), 335 nm ( $R = 45.0$ ), 317 nm ( $R = 69.6$ ), 310 nm ( $R = -74.7$ ), 293.5 nm ( $R = 74.2$ ), and 293.1 nm ( $R = -79.8$ ). In addition, the overall intensity of  $\text{Au}_{11}(\text{PH}_3)_8\text{Cl}_2^+$  is approximately one-fourth that of  $\text{Au}_{11}(\text{dpb})_4\text{Cl}_2^+$ . The  $C_2$  structure of  $\text{Au}_{11}(\text{PH}_3)_8\text{Cl}_2^+$ , which lies 21.74 kJ/mol higher than the global minimum, has a CD spectrum (Figure 9b) with overall intensities approximately twice those of the lowest energy  $C_1$  structure, which suggests that higher-order chiral symmetries may lead to large CD signals. It is important to note that although  $\text{Au}_{11}(\text{PH}_3)_8\text{Cl}_2^+$  has a nonzero CD spectrum, it is implausible for this system to exhibit positive and negative Cotton effects in experiment because the mirror image enantiomer should be present in the same concentration; furthermore, the expected fluxionality of the species may lead to equal concentrations of the two enantiomers due to rearrangement of the gold core at room temperature even if a chiral separation procedure is undertaken. In contrast, the mirror image enantiomer of  $\text{Au}_{11}(\text{S-dpb})_4\text{Cl}_2^+$  is only formed when R-dpb is used in the synthesis of the compound. The structure and CD spectrum of  $\text{Au}_{11}(\text{R-dpb})_4\text{Cl}_2^+$  are shown in Figure S1 and are mirror images of those for the S-conformer.

**Comparison of  $\text{Au}_{11}(\text{dpb})_4\text{Cl}_2^+$ ,  $\text{Au}_{11}\text{Cl}_2^+$ , and  $\text{Au}_{11}^{3+}$ .** The differences between the CD spectra and rotatory strengths of the  $\text{Au}_{11}(\text{dpb})_4\text{Cl}_2^+$  and  $\text{Au}_{11}(\text{PH}_3)_8\text{Cl}_2^+$  systems suggest that the ligands themselves may also play a role in the intensities in the CD spectrum. Without reoptimization, dpb ligands have been removed from the  $\text{Au}_{11}(\text{dpb})_4\text{Cl}_2^+$  structure and CD spectra have been calculated for the  $\text{Au}_{11}\text{Cl}_2^+$  and  $\text{Au}_{11}^{3+}$  subsystems (Figure S2 in the Supporting Information). The intensities of the resulting transitions are much weaker than those for  $\text{Au}_{11}(\text{dpb})_4\text{Cl}_2^+$ , which shows that ligands contribute dramatically to the strong chiroptical effects. The largest rotatory strengths observed for  $\text{Au}_{11}\text{Cl}_2^+$  and  $\text{Au}_{11}^{3+}$  are 27.9 and 18.3  $10^{-40}$  esu<sup>2</sup> cm<sup>2</sup>, respectively, which are less than a fifth of the largest rotatory strengths for the complex with dpb ligands. Again, the primary transitions arise from excitations within delocalized metal superatom orbitals. The Kohn–Sham orbitals of these systems similarly show P-like and D-like character. So, although the low-energy transitions for each of these systems have metal–metal character, the presence of bidentate phosphine ligands increases the chiroptical signal. This supports the model of Beratan et al. that suggests that even symmetric metal cores can be optically active when perturbed by a dissymmetric field originating from the adsorbates.<sup>12</sup>



## Conclusions

The theoretical CD spectrum of  $\text{Au}_2\text{Br}_2\text{BINAP}$  agrees with experiment to within approximately 10 nm. The  $\text{Au}_2\text{Cl}_2\text{BINAP}$  CD spectrum is very similar to its bromide analog. Replacement of BINAP by the model bidentate phosphine ligand dpb affects the CD spectrum of  $\text{Au}_2\text{X}_2\text{L}$  at wavelengths shorter than 350 nm.

The lowest energy structure of  $\text{Au}_{11}(\text{dpb})_4\text{X}_2^+$  has a chiral  $C_2$  geometry, so it is more symmetrical than the related  $\text{Au}_{11}(\text{PH}_3)_8\text{Cl}_2^+$  system with a  $C_1$  core. The theoretical  $\text{Au}_{11}(\text{dpb})_4\text{X}_2^+$  CD spectrum of this complex has two large negative peaks around 480–530 nm and 390–410 nm, which closely match experiment (within the usual underestimation). The third peak in the spectrum at 300–350 nm has the opposite sign from experiment; this is presumably due to substitution of BINAP by the model ligand dpb.

The superatom model holds for the  $\text{Au}_{11}(\text{dpb})_4\text{X}_2^+$  complex; the three highest occupied Kohn–Sham orbitals are P-like and several of the unoccupied orbitals have D-like character. The absorption and CD spectra are dominated by metal–metal transitions in the low-energy peaks. Even though these transitions are metal-based, ligands have a strong effect on intensities of CD signals; the rotatory strengths calculated for  $\text{Au}_{11}(\text{PH}_3)_8\text{Cl}_2^+$  ( $C_1$  core),  $\text{Au}_{11}\text{Cl}_2^+$  (frozen  $C_2$  core), and  $\text{Au}_{11}^{3+}$  (frozen  $C_2$  core) are much smaller than those computed for

$\text{Au}_{11}(\text{dpb})_4\text{Cl}_2^+$ . Overall, reduction of the core chiral symmetry from  $C_2$  to  $C_1$  leads to a decrease in the rotatory strengths by a factor of 2, whereas removal of the ligands results in a decrease of approximately 5–10 for this system. Thus, bidentate phosphine ligands such as BINAP and dpb lead to effects on both the core structure and the CD spectrum. This study is the first to clearly show that the optical activity of the metal core is very sensitive to the existence and chiral arrangement of the surrounding ligands.

**Acknowledgment.** We thank Prof. Tsukuda for sending experimental optical absorption and circular dichroism data for the  $\text{Au}_{11}(\text{BINAP})_4\text{X}_2^+$  and  $\text{Au}_2\text{X}_2\text{BINAP}$  compounds from ref 25. We thank Prof. Hannu Häkkinen for discussions related to the  $\text{Au}_{11}\text{Cl}_2^+$  system. C.M.A. acknowledges start-up and seed funding from Kansas State University.

**Supporting Information Available:** Bond distances for  $\text{Au}_2\text{X}_2\text{L}$ . Wavelengths, rotatory strengths, and single-particle transitions and their weightings for excitations below 395 nm in the CD spectrum of  $\text{Au}_{11}(\text{S-dpb})_4\text{Cl}_2^+$ , CD spectra of  $\text{Au}_{11}(\text{R-dpb})_4\text{Cl}_2^+$ ,  $\text{Au}_{11}\text{Cl}_2^+$ , and  $\text{Au}_{11}^{3+}$  complexes. This material is available free of charge via the Internet at <http://pubs.acs.org>.

JA906884M